Modelling acid stimulation in the enhanced geothermal system of Soultz-sous-Forêts (Alsace, France)

Yann Lucas*, Viet V. Ngo, Alain Clément, Bertrand Fritz, Gerhard Schäfer

Université de Strasbourg, CNRS, LHyGeS UMR 7517, Strasbourg, France

ABSTRACT

The Soultz-sous-Forêts geothermal plant in northern Alsace (France) is under consideration for a campaign to actively stimulate the low-permeability granitic reservoir. The operation of the enhanced geothermal system requires the re-injection of fluid into the geothermal reservoir, which can cause a strong disequilibrium between the fluid and the granitic rock, as well as the possible dissolution/precipitation of minerals. These mineralogical transformations may have a significant impact on porosity, permeability and fluid pathways in the geothermal reservoir. Various studies have reported that the hydraulic connection between the injection well and the production well is quite poor. Therefore, chemical stimulations are necessary to increase the productivity and injectivity of the Soultz geothermal system.

Before performing chemical stimulation in the Soultz geothermal system, a modelling approach is considered to discuss different scenarios in terms of the choice of acid and the amount and duration of acid injection. The approach used in this work is based on the geochemical code KIRMAT, which enables us to represent the geothermal reservoir using single-porosity and double-porosity models. The code evaluates the changes in the porosity and permeability of the Soultz reservoir based on the evolution of all primary and secondary minerals as a function of time in the geothermal system.

The modelling results showed that chemical stimulation could significantly increase porosity and permeability; however, for both single and double-porosity models, the improved zones are very limited and are only present within a few meters of the reinjection well. The modelling results obtained from the sensitivity case studies showed the significant impact of the Darcy velocity, the initial concentration of the acid used, the duration of the injection and the initial calcite amount, especially in regard to the changes in porosity and the mineralogical transformation of the zone around the acid-injected well. Higher concentrations of the HCl solution also increase the dissolution of primary minerals and then exhibit a stronger porosity increase in the zone around the injection well, but further, precipitation reduces the positive achievements of chemical stimulation.

1. Introduction

The Upper Rhine Graben is known for a long time for its high geothermal gradient (Haas and Hoffmann, 1929) and the Soultz-sous-Forêts site, located in Northern Alsace (France), was chosen 30 years ago as a geothermal pilot research site and became an Enhanced Geothermal System (EGS) demonstrator. It nowadays consists of three active wells, called GPK2, GPK3, and GPK4, in which GPK2 and GPK4 are re-injection wells and GPK3 the production well. These wells are drilled down to 5000 m and are active in the granite basement rock. This deep Paleozoic granitic basement lies at a depth of 1400 m at Soultz-sous-Forêts, covered by a Permo-Triassic clastic formation (Aichholzer et al., 2016), which plays an important role in the hydrothermal convection at

the regional scale (Heap et al., 2017). In the present study, what is at stake for the geothermal exploitation, it is the poor hydraulic connection and the low natural permeability of granite (Genter et al., 2010), and it implies hydraulic and/or chemical stimulation to achieve a fluid rate high enough for energy production. Currently, the Soultz-sous-Forêts geothermal plant is under consideration for a campaign to actively stimulate the low-permeability granitic reservoir.

Acid stimulation is comprised of a so-called soft-stimulation treatment, whereby some combination of acids, chelating agents and/or retarding agents are injected or otherwise introduced into the open-hole section of a geothermal well, with the ultimate aim of increasing rock permeability whilst avoiding the generation of detectable seismicity. To allow for the operation of the enhanced geothermal system,

---

(EGS) the re-injection of fluid into the geothermal reservoir is necessary, which can cause a strong thermodynamic disequilibrium between the fluid and the granitic rock within a geothermal reservoir, which then implies possible dissolution/precipitation (Fritz et al., 2010; Ngo et al., 2016). In the Soultz-sous-Forêts EGS, hydrothermal alterations include the transformation of plagioclase, biotite and K-feldspar and the precipitation of various secondary minerals. The major sealing phases observed in the main fracture zones are quartz, calcite, and clay minerals (e.g., Ledésert et al., 1999; Bartier et al., 2008; Hébert et al., 2010). These mineralogical transformations may have a significant impact on the porosity, permeability and fluid pathways of the geothermal reservoir. A literature review revealed that the hydraulic connection between the injection well and the production well is historically quite poor (GEIE EMC, 2017). Therefore, chemical stimulations are required in order to increase the productivity and injectivity of the Soultz geothermal system.

Chemical stimulation is a method where a certain volume of chemicals (or a mixture of chemicals) is injected into a geothermal reservoir. This method aims to improve or maintain well productivity/injectivity without damaging the host rock by: full or partial dissolution of minerals, mobilisation of reservoir particles in fractures and pores, inhibition of secondary or tertiary reaction products that are sparingly soluble, and controlling the reactivity of mineral surfaces (GEIE EMC, 2017). In the context of the Soultz geothermal reservoir, different types of chemicals were injected and tested for their efficiency. These include conventional acid systems such as HCl and a HCl-HF mixture, chelating agents such as Nitrilotriacetic Acid (NTA) and retarded acid systems such as Organic Clay Acid (OCA) and Rock Mud Acid (RMA). The outcome of chemical stimulation depends on many factors, including the type and concentration of injected chemicals, the injection pressure, flow rates, the fracturing pressure of the host rock, casing damages, mobilisation of cuttings, fines and drilling residues, and precipitation of non-welcome secondary reaction products (Nami et al., 2008; Portier et al., 2009).

In geothermal systems, acidizing stimulation is expected to affect the target zone around the injection well as much as possible, and therefore should penetrate more deeply into the formation via fracture zones with pre-existing secondary mineralogy. At the Soultz geothermal site, the natural fractures are very heterogeneous and irregularly localized (Ledésert et al., 1993a). This causes the different hydraulic characteristics of the fractures, and hence makes an acidizing operation challenging in regard to the effective distribution of chemicals. Before performing chemical stimulation in the Soultz geothermal system, a modelling approach is considered in order to discuss different scenarios in terms of the choice of acid, and the amount and duration of acid injection.

The approach used in this work is based on the geochemical numerical code KIRMAT, which enables us to represent the geothermal reservoir using single and double porosity models and account for a wide range of mineralogy. The model evaluates changes in porosity and permeability in the geothermal reservoir based on changes in the amount of primary and secondary minerals as a function of time in the geothermal system.

2. Materials and methods

2.1. The numerical reactive transport model

2.1.1. Governing equations of reactive mass transport

The hydrochemical model developed in this study is based on the numerical code KIRMAT (Kinetic Reaction and Mass Transport) (Gérard, 1996), which combines geochemical reactions and 1D mass transport equations. The mass balance equation of reactive transport in a one-dimensional porous medium is written as (Lichtner, 1988; Gérard et al., 1998):

$$\frac{\partial}{\partial t}(\phi \Psi_j) = \phi D\left(\frac{\partial^2 \Psi_j}{\partial x^2}\right) - U\frac{\partial \Psi_j}{\partial x} - \sum_{r=1}^{M} \alpha_{jr}\frac{\partial}{\partial t}(\phi_r \widetilde{V}_r^{-1}) (j=1, ...,N) \tag{1}$$

and

$$\frac{\partial}{\partial t}(\phi_r \widetilde{V}_r^{-1}) = v_r (r=1, ...,M) \tag{2}$$

where Eq. (1) refers to N aqueous primary species and Eq. (2) refers to M primary species of reacting minerals. In these equations, Ψ_j denotes the generalized (or total) concentrations (in moles per water mass or volume) of primary species, ϕ denotes the porosity of the porous medium, ϕ_r and α_{jr} denote the volume fraction and the stoichiometric reaction coefficients, respectively, of the rth mineral with molar volume $\widetilde{V}_r$, v_r represents the reaction rates of the irreversible reaction of minerals and fluids equivalent to the rate of precipitation or dissolution of reacting minerals r per unit of the rock and fluid system (by convention, v_r is positive for precipitation and negative for dissolution reactions), D denotes the hydrodynamic dispersion coefficient, and U denotes the Darcy velocity. x is the space variable and t is the time. In Eq. (3), the generalized concentration Ψ_j is defined according to the expression:

$$\Psi_j = C_j + \sum_i \alpha_{ji}C_i, \text{with} C_i = K_i\gamma_i^{-1}\prod_{j=1}^{N}(\gamma_j C_j)^{\alpha_{ji}} \tag{3}$$

where C_j refers to the concentration of the jth primary species, and the sum runs over all aqueous secondary species with concentration C_i related to the concentrations of the primary species through the mass action equation. The quantity α_{ji} denotes the molar stoichiometric coefficient of species j in secondary species i, γ is the activity coefficient of the aqueous species, and K_i denotes the equilibrium constant. Using Eqs. (1) and (2), one obtains a system of (N + M) coupled nonlinear partial differential equations.

In the case of a double-porosity medium, divided between the matrix and a fractured medium, the mass balance equations of reactive transport are written as: in a fractured medium:

$$\frac{\partial}{\partial t}(\phi^f \Psi_j^f) = \phi^f D\left(\frac{\partial^2 \Psi_j^f}{\partial x^2}\right) - U\frac{\partial \Psi_j^f}{\partial x} + \varphi_j^f + \frac{\alpha}{e}\phi^f D_{diff}(\Psi_j^m - \Psi_j^f)(j=1, ...,N) \tag{4}$$

in the matrix, where it is assumed that no flow and no mass transport take place,

$$\frac{\partial}{\partial t}(\phi^m \Psi_j^m) = \varphi_j^m - \frac{\alpha}{e}\phi^m D_{diff}(\Psi_j^m - \Psi_j^f)(j=1, ...,N) \tag{5}$$

where Ψ_j^f and Ψ_j^m are the dissolved global concentrations of primary species j in fractured medium and matrix, respectively (mol.L^{-3}); ϕ^f and ϕ^m are the porosity of fractured medium and matrix, respectively (L^3.L^{-3}); D is the effective hydrodynamic dispersion coefficient (L^2.T^{-1}) in fractures; D$_{diff}$ is the diffusion coefficient (L^2.T^{-1}) in matrix; U is the Darcy velocity (L.T^{-1}); φ_j^f and φ_j^m are the sink terms corresponding to the geochemical fluxes in fractured medium and matrix, respectively (mole.L^{-3}.T^{-1}); α is the surface contact between fractured medium and matrix (L^2); e is the volume contact between fractured medium and matrix (L^3).

KIRMAT aims to contribute to the understanding of water-rock interactions in different frameworks as groundwater salinization (Lucas et al., 2010; M'Nassri et al., 2019), weathering processes (Lucas et al., 2017; Ackerer et al., 2018) or hydrothermal alteration (Ngo et al., 2016). It can also be used to simulate clay minerals evolution under specific environmental conditions, such as the storage of nuclear waste (Montes et al., 2005a; 2005b; Marty et al., 2009, 2010, 2006; Ngo et al., 2014).

2.1.2. Water-rock interactions

In KIRMAT, interactions between water and rock involve dissolution and precipitation. In our study, only mineral dissolution is modelled by
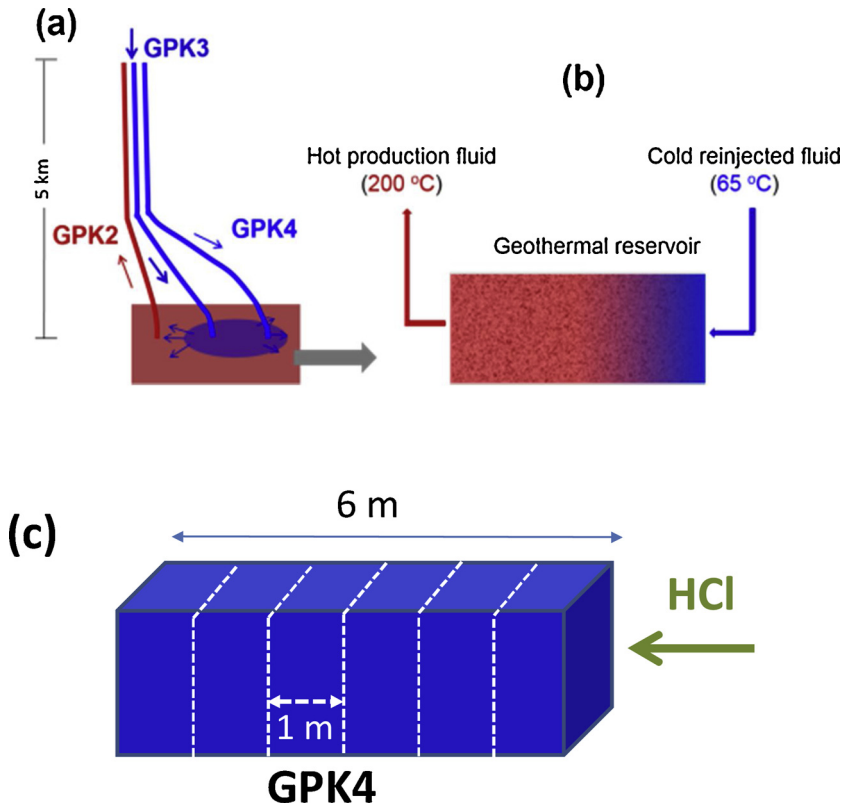
(a)

(b)

(c)

Fig. 1. Conceptual schema of the stimulated Soultz geothermal system: (a) Cross-section of the Soultz EGS system (Alsace, France), GPK2 is the production well, while GPK3 and GPK4 are the re-injection wells; (b) conceptual model with the re-injection well ($\approx 65\ °C$) and the production well ($\approx 200\ °C$); (c) model domain used in KIRMAT simulations.

irreversible kinetics, while precipitation is modelled at equilibrium. Kinetic rock dissolution rate r_d (in mole per water mass) is quantified by (Gérard, 1996):

$$r_d \equiv v_r = k_{d,r} S_r^{eff} \alpha_{H^+}^n \left(1 - \left(\frac{Q_r}{K_r} \right)^{n1} \right)^{n2}$$

(6)

where $k_{d,r}$ denotes the dissolution rate constant (mol. m^{-2}. $year^{-1}$) of the reactive mineral r, S_r^{eff} stands for the reactive surface area of mineral r (m^2.kg_{H2O}^{-1}), $\alpha_{H^+}^n$ denotes the proton activity where n depends on the pH of the solution, n_1 and n_2 are exponents depending on the pH of the solution, Q_r is the ion activity product of reactive mineral r and K_r denotes the thermodynamic equilibrium constant of the hydrolysis reaction of mineral r at a given temperature and pressure.

The KIRMAT code can describe the feedback effect of the chemical and mineralogical evolution of porosity and permeability at any node of the mesh due to dissolution and precipitation reactions. In Eq. (7) the intrinsic permeability k (m^2) is updated after each time step as follows (Gérard, 1996):

$$k = C_0 \left[\phi^{C-1} \left(\frac{\phi^3}{(1-\phi)^2 S^2} \right) \right]^2$$

(7)

where C_0, ϕ, C and S denote an experimental constant, the porosity of the porous medium, the cementation factor, and the grid cell surface in contact with the adjacent cell (m^2), respectively.

In Eq. (8) the relationship of the effective diffusion coefficient (D_{diff}) to the porosity is expressed as:

$$D_{diff} = D_0 \phi^{C-1}$$

(8)

where D_0 is the diffusion coefficient of the solute in free water, ϕ is the porosity, and C the cementation factor.

In Eq. (9) the porosity at the time increment n is determined as follows:

$$\phi^n = 1 - \left[\frac{S\Delta x(1 - \phi^{n-1}) + Bv^n}{S\Delta x} \right]$$

(9)

where ϕ^n and ϕ^{n-1} are the porosities at the time increments n and n-1, respectively; Δx is the cell length (m) and Bv^n is the absolute volume balance of all minerals at time increment n (m^3).

2.2. Acid stimulation of the geothermal reservoir

2.2.1. Conceptual system

The acid stimulation method is applied to geothermal reservoirs for a few decades. This approach is generally expensive and complicated, and its success depends on many factors. Gathering knowledge about the well that is chosen for acid stimulation is the first task that should be thoroughly performed. The next step is to select a suitable chemical and/or a mixture of chemicals. When applying the acid stimulation, the acid solution can be injected stepwise into the geothermal reservoir using different steps, known as pre-, main- and post-flush. Each step needs to be designed and balanced carefully against the rest to achieve its own objective (GEIE EMC, 2017).

The GPK-4 well actually has a very poor connection with other wells in the Soultz system. According to the feasibility study completed recently by the GEIE Exploitation Minière de la Chaleur (GEIE EMC, 2017), the GPK-4 injection well is considered to be the most appropriate well for acid stimulation based on the evaluation of the technical and economic feasibility. Therefore, in the current modelling work, we assumed that well GKP-4 would be chosen for acid stimulation. Acid stimulation of well GPK-4 is expected to improve its connection with other wells, as well as improving the overall hydraulic regime of the Soultz system.

Knowledge about the reservoir petrology and fracture filling mineralogy is crucial for selecting a chemical. Additionally, other factors include which minerals need to be dissolved and if a composition of native brine and injection setup should be used also need to be considered to coordinate the best efficiency of the injected products and avoid unwelcome secondary reactions (GEIE EMC, 2017). The results

obtained for previous acid stimulations in the Soultz system have shown that with a HCl solution, the carbonate minerals present in the deep reservoirs of wells GPK-2, GPK-3 and GPK-4 could be successfully removed by injecting an acid solution with a concentration up to 0.45 % (Nami et al., 2008; Portier et al., 2009). Therefore, for this modelling work, the simple and inexpensive acid HCl will be tested. This simple acid was chosen, since it has a fast and strong dissolution effect and reacts with minerals quickly when it comes into contact with the system. Otherwise, it is also expected that a simple stimulation fluid can keep the environmental footprint of the stimulation operation as low as possible.

Fig. 1 represents a conceptual system of the Soultz geothermal reservoir, where the thermal cycle of the fluid occurs between 200 °C and 65 °C in the geothermal loop (André et al., 2006; Fritz et al., 2010). The system consists of a 6 m thick layer initially saturated by water at 65 °C. The temperature value of 65 °C in the geothermal reservoir near the injection well was considered to be a constant value during the stimulation process. The injected acid solution is assumed to be heated up to 65 °C and allowed to penetrate in the near field around the stimulation well. This simple approach of the transition between the stimulated acid solution and the Soultz geothermal reservoir used as the boundary condition will simplify the calculated chemical speciation. The conduction of heat in the system is not considered herein.

For the current work, the computation time was quite long, meaning that depending on the modelling case, it may take several months to accomplish one numerical simulation. We further acknowledge that the cell size may also have an impact on the modelling output when using the geochemical modelling code as reported in several modelling studies (Marty et al., 2009; Ngo et al., 2014). In the current work, we therefore attempted to evaluate the effects of cell size on the modelling results with different sizes as 0.1 m, 0.2 m, 0.5 m and 1 m, together with different lengths of the system, including 6 m, 10 m and 20 m. The different outputs were more or less different but not significantly, so they are not presented, and a cell size of 1 m and a length of 6 m were chosen as the default values because of the reasonably clear results and the computation time.

In the present work, special attention was paid to evaluate the impact of the injection conditions and the reservoir conditions on the evolution of the reservoir after the acid stimulation. There are two reasons that inspire us to focus on these issues. First, as discussed previously, the appropriateness of the injection conditions generally plays a critical role in the stimulation results. Second, depending on the geothermal reservoir properties, the capacity of the acid solution to penetrate into the geothermal reservoir and the interaction between the acid solution and different minerals in the reservoir must be different.

2.2.2. Modelling approach

In the framework of the single porosity model, a reference case was used for the input data presented in Tables 1–5. These data were collected from a literature review. Additionally, HCl concentration was 0.2 % (pH = 0.74), and injection duration was 2 days with a Darcy velocity of 1 m.h^{-1}. Three sensitivity cases were tested. It is important to highlight that the input data are the same for all three cases except for the tested sensitivity parameters. The numerical calculations performed in this way are able to distinguish the effects of the tested parameters on the evolution tendency of the system.

For the modelling tests using the double porosity model, the matrix and fracture fractions are presented separately by their own mineralogical compositions and physical properties such as porosity and permeability. Two modelling cases are conducted and the only difference between them is the parameter representing the ratio of surface contact to volume contact between the matrix and fracture zones (parameter $\frac{\alpha}{e}$ in Eqs. (4) and (5)). The comments and discussion of the modelling results are mainly based on two criteria, porosity and permeability.

Table 1

Main mineralogical compositions, corresponding volume fractions and the estimated reactive surface areas of the Soultz granite considered in the current modelling work. The volume fraction values were taken from those in Jacquot (2000) and based on the assumption that the fresh granite contains 90 % of the volume fraction and the rest is vein alteration.

Minerals[a]	Structural formula	Volume fraction (%)	Reactive surface area (m^2 kg^{-1}H$_2$O)
Quartz	SiO$_2$	25.87	308.30
K-Feldspar	KAlSi$_3$O$_8$	22.63	7457.55
Albite	NaAlSi$_3$O$_8$	36.25	8262.75
Anorthite	Ca(Al$_2$Si$_2$)O$_8$	2.00	124.21
K-Muscovite	KAl$_2$(AlSi$_3$)O$_{10}$(OH)$_2$	2.82	631.77
Annite	KFe$_3$(AlSi$_3$)O$_{10}$(OH)$_2$	2.82	740.82
Phlogopite	KMg$_3$(AlSi$_3$)O$_{10}$(OH)$_2$	2.82	622.69
Calcite	CaCO$_3$	0.46	112.19
Mg-Illite	K$_{0.85}$Mg$_{0.25}$Al$_{2.35}$Si$_{3.4}$O$_{10}$(OH)$_2$	0.87	6375.75
Fe-Illite	K$_{0.85}$Fe$_{0.25}$Al$_{2.35}$Si$_{3.4}$O$_{10}$(OH)$_2$	0.87	6687.79
Al-Illite	K$_{0.85}$Al$_{2.85}$Si$_{3.15}$O$_{10}$(OH)$_2$	0.87	6611.52
Smectite	[Ca$_{0.009}$Na$_{0.409}$K$_{0.024}$] [(Si$_{3.738}$Al$_{0.262}$] [Al$_{1.598}$Fe$_{0.208}$Mg$_{0.214}$]O$_{10}$(OH)$_2$	0.97	5484.20
Dolomite	CaMg(CO$_3$)$_2$	0.08	20.71
Chamosite	Fe$_5$Al(AlSi$_3$)O$_{10}$(OH)$_8$	0.33	13.72
Clinochlore	Mg$_5$Al(AlSi$_3$)O$_{10}$(OH)$_8$	0.33	10.79
Physical properties			
Porosity			5 %
Permeability			10^{-16} m^2

[a] Plagioclase was replaced by Albite and Anorthite; Micas by Muscovite. Annite and Phlogopite. and Chlorite by Chamosite and Clinochlore.

Table 2

Main mineralogical composition, volume fraction and estimated reactive surface area of the matrix and facture Soultz granite considered in the current modelling work. The volume fraction values were taken from those in Jacquot (2000).

Minerals	Matrix		Fracture		
	Volume fraction (%)	Reactive surface area (m^2 kg^{-1}H$_2$O)	Minerals	Volume fraction (%)	Reactive surface area (m^2 kg^{-1}H$_2$O)
Quartz	24.2	288.40	Quartz	40.9	487.42
K-Feldspar	23.6	7777.20	K-Feldspar	13.9	4580.64
Albite	40.5	9231.49	Calcite	3.9	951.17
Anorthite	2	124.21	Mg-Illite	8.7	63757.49
Muscovite	3.13	701.22	Fe-Illite	8.7	66877.88
Annite	3.13	822.26	Al-Illite	8.7	66115.20
Phlogopite	3.13	691.15	Smectite	9.7	54841.96
Calcite	0.3	73.17	Dolomite	0.8	207.06
			Chamosite	2.4	137.19
			Clinochlore	2.4	107.86
Physical properties			**Physical properties**		
Porosity	10 %		Porosity	1 %	
Permeability	10^{-16} m^2		Permeability	10^{-14} m^2	

2.3. Initial conditions

2.3.1. Mineralogical composition of the Soultz geothermal reservoir

As a potential host rock for an enhanced geothermal system, the Soultz system is the subject of many experimental and theoretical investigations (e.g., Ledésert et al., 1993a, b, 1999, 2009, 2010; Dubois et al., 1996, 2000; Sausse, 2002; Baldeyrou et al., 2003; Baldeyrou-Bailly et al., 2004; Sausse et al., 2006; Bartier et al., 2008; Hébert et al., 2010, 2011; Hébert and Ledésert, 2012), as well as modelling studies (e.g., Komninou and Yardley, 1997; Rabemanana et al., 2003; Bächler

Table 3
pH, Eh and chemical composition of the equilibrated solution of the Soultz geothermal reservoir at 65 °C.

pH	5.39
Eh (mV)	−171
p_{CO2} (atm)	4.7×10^{-2}

Elements	Concentration (mol kg^{-1}H$_2$O)
K	8.31×10^{-2}
Na	1.21×10^{0}
Ca	1.35×10^{-1}
Mg	5.14×10^{-3}
Si	2.20×10^{-4}
Al	3.92×10^{-8}
Fe	1.00×10^{-5}
Pb	1.48×10^{-6}
S	1.23×10^{-10}
Cl	1.56×10^{0}
C	3.74×10^{-2}
Alkalinity (eq kg^{-1}H$_2$O)	1.0×10^{-2}

Table 4
Thermodynamic database of the primary minerals in the Soultz granite and secondary minerals tested in the current study. The thermodynamic constants at different temperatures were taken from the Thermoddem database (Blanc et al., 2012).

Minerals	Structural formula	Molar volume (cm^3 mol^{-1})	LogK65 °C (-)
Primary minerals			
Quartz	SiO_2	22.69	−3.30
K-Feldspar	$K(AlSi_3)O_8$	108.74	−1.13
Albite	$NaAlSi_3O_8$	100.07	1.01
Anorthite	$Ca(Al_2Si_2)O_8$	100.79	18.83
K-Muscovite	$KAl_2(AlSi_3)O_{10}(OH)_2$	140.81	8.26
Annite	$KFe_3(AlSi_3)O_{10}(OH)_2$	154.32	26.28
Phlogopite	$KMg_3(AlSi_3)O_{10}(OH)_2$	149.66	33.66
Calcite	$CaCO_3$	36.93	1.26
Mg-Illite	$K_{0.85}Mg_{0.25}Al_{2.35}Si_{3.4}O_{10}(OH)_2$	140.25	5.67
Fe-Illite	$K_{0.85}Fe_{0.25}Al_{2.35}Si_{3.4}O_{10}(OH)_2$	140.53	4.34
Al-Illite	$K_{0.85}Al_{2.85}Si_{3.15}O_{10}(OH)_2$	139.49	6.18
Smectite	$[Ca_{0.009}Na_{0.409}K_{0.024}]$ $[(Si_{3.738}Al_{0.262}]Al_{1.598}Fe_{0.208}Mg_{0.214}]$ $O_{10}(OH)_2$	134.92	1.45
Dolomite	$CaMg(CO_3)_2$	64.12	2.06
Chamosite	$Fe_5Al(AlSi_3)O_{10}(OH)_8$	215.88	37.17
Clinochlore	$Mg_5Al(AlSi_3)O_{10}(OH)_8$	211.47	49.33
Secondary minerals			
FeIII-Illite	$K_{0.85}Fe_{0.25}^{III}Al_{2.6}Si_{3.15}O_{10}(OH)_2$	140.56	5.98
K-Beidellite	$K_{0.34}Al_{2.34}Si_{3.66}O_{10}(OH)_2$	134.15	0.48
Ca-Saponite	$Ca_{0.17}Mg_3Al_{0.34}Si_{3.66}O_{10}(OH)_2$	138.84	23.26
FeCa-Saponite	$Ca_{0.17}Mg_2FeAl_{0.34}Si_{3.66}O_{10}(OH)_2$	139.96	21.86
Siderite	$FeCO_3$	29.38	−0.83
Ankerite	$CAFe(CO_3)_2$	70.79	1.04
Anhydrite	$CaSO_4$	45.94	−4.88

and Kohl, 2005; André et al., 2006; Fritz et al., 2010; Ngo et al., 2016). Various studies have reported that the mineralogy of the Soultz geothermal reservoir is very heterogeneous (e.g., Genter, 1989; Hébert et al., 2010). The heterogeneity, which depends on the location, comes from the fact that the fractions of fresh and altered granites are variable. Furthermore, there is a clear difference between the so-called fresh granites in the Soultz reservoir. For example, fresh granite mainly contains minerals such as K-feldspar, plagioclase, quartz, and biotite, while altered granite is generally comprised of quartz, K-feldspar, illite, smectite, mica, calcite, dolomite, pyrite, galena, and chlorite (e.g., Ledésert et al., 1999; Bartier et al., 2008; Hébert et al., 2010). A literature review reveals that the main secondary minerals in the Soultz

reservoir are carbonates and illite/smectite. Depending on the degree of the fluid-rock interaction, the volume fraction of these newly formed minerals in the altered granite and vein alteration can reach approximately 50 %.

As noted previously, the GPK-4 injection well was selected to apply the acid stimulation. The literature review shows that the fracture mineralogy of this well may have similar characteristics to the fracture zones of the upper and intermediate reservoir in terms of secondary fracture mineralization of quartz, calcite, illite, chlorite, sulfides, barite and haematite (Genter and Traineau, 1992; Dezayes et al., 2005). The dataset presented in the thesis of Jacquot (Jacquot, 2000) was chosen to describe the minerals that were initially present in the Soultz geothermal reservoir. Additionally, to estimate the volume fraction of each mineral, we assumed that the fractions of fresh and altered granites are 90 % and 10 %, respectively. Tables 1 and 2 present the composition and corresponding volume fraction of primary minerals for the single-porosity and double porosity models, respectively. To fit with the Thermoddem database (Blanc et al., 2012), several groups of minerals are represented by the most typical minerals in their group: plagioclase was replaced by albite and anorthite end-members; K-muscovite, annite, and phlogopite were used for mica; chlorite was represented by clinochlore and chamosite end-members; and illites are represented using three different compounds, known as Fe-illite, Mg-illite, and Al-illite.

The study of Surma and Géraud (2003) that is based on rock samples taken in bore hole EPS1 located in the neighborhood of GPK4 showed that the porosity can vary from 0.3%–10%. In Géraud et al. (2010), based on samples of the same zone, the lowest values of porosity are between 0.5 and 1 %, but can reach 15 % in the fault zone. Villeneuve et al. (2018) also found porosities varying between 0.09 and 0.3 %. For a single-porosity model that encompasses fractured and non-fractured zone, we consider that 5 % represent an average porosity. In a double-porosity model, the matrix porosity is generally considered much higher than the porosity of the fracture. Our choice of respectively 10 and 1 % represent two end-members with a significant difference of order of magnitude. Concerning the permeability of the rock, the estimations of Sausse et al. (2006) performed in GPK1 between 2849 and 3100 m depth vary from 8.6 10^{-18} to 9.6 10^{-16} m^2. In addition, the later work of Vogt et al. (2012) indicates that 10^{-16} and 10^{-14} m^2 are two values that frame rather well the permeability of the hydrosystem. For our single-porosity model we thus consider that 10^{-16} m^2 can represent the average permeability in a good approximation. In the case of a double-porosity model, the matrix permeability is generally much lower than the fracture permeability. Our choice of respectively 10^{-16} and 10^{-14} m^2 represents two end-members with a significant difference of order of magnitude.

2.3.2. Pore-water composition

Reference pore-water composition and its evolution over time have to be estimated for the assessment of general performance. Generally, pH is considered as a key parameter of pore-water composition because it has important effects on the reactions in geothermal reservoirs. The pH of the geological fluid depends on the interaction of a variety of factors, such as the ion exchange of clay and the dissolution-precipitation reactions of trace carbonate minerals and major clay mineral components. In this work, the THERMA code (Ngo et al., 2016) was applied to determine the pore-water composition of the Soultz geothermal reservoir at 65 °C. The chemical composition of geological fluid in equilibrium with the geothermal reservoir at 65 °C is presented in Table 3. The input data for the THERMA code are taken from laboratory analyses of fluid collected from the production well head (Sanjuan et al., 2006; Scheiber et al., 2013) and from thermodynamic modelling (Sanjuan et al., 2006; Fritz et al., 2010; Ngo et al., 2016). The details regarding the modelling work completed using the THERMA code can be found in Ngo et al. (2016). The pH value of 5.39 is higher than the value of 4.8 of the saline fluid measured *in situ* at the well-heads

Table 5

Kinetic constants of dissolution reactions of the primary minerals in the Soultz geothermal reservoir at 25 °C. The kinetic constant values at 65 °C are extrapolated using the activated energy.

Minerals	k_a (mol m^{-2} year^{-1})	k_n	k_b	pH$_a$	pH$_b$	n_a	n_b	E$_a$ (KJ mol^{-1})	E$_n$	E$_b$
25 °C										
Quartz	1.44E-4[a]	1.44E-6[b]	1.62E-9[b]	4.0[a]	5.9[b]	0.50[a]	−0.50[b]	99.2[a,b]	90.1[b]	108.4[b]
K-Feldspar	2.75E-3[b]	1.23E-5[b]	1.99E-14[b]	4.7	10.7	0.5	−0.82	51.7	38.0	94.1
Albite	2.18E-3[b]	8.66E-6[b]	7.91E-9[b]	6[a]	8[a]	0.46	−0.57	65.0	69.8	71.0
Anorthite	9.95E+3[b]	2.39E-2[b]	7.91E-9[b]	6[a]	8[a]	1.41	−0.57	16.6	17.8	22.0
Muscovite	4.44E-5[b]	8.88E-6[b]	8.88E-8[b]	6[a]	8[a]	0.37	−0.22	22.0	22.0	22.0
Annite	4.60E-3[b]	8.88E-6[b]	8.88E-8[b]	6[a]	8[a]	0.53	−0.22	22.0	22.0	22.0
Phlogopite	4.44E-5[b]	1.25E5[b]	8.88E-8[b]	6[a]	8[a]	0.37	−0.22	22.0	29.0	23.5
Calcite	1.58E+7[b]	4.88E+1[b]	4.88E+1[a]	5.5[b]	8.0[a]	1.00[b]	0[a]	14.5[b]	23.5[b]	23.5[a,b]
Mg-Illite	6.29E-5[d]	6.29E-8[d]	3.15E-13[d]	5.0[d]	8.8[d]	0.60[d]	−0.60[d]	46[a,d,e]	14[a,d,e]	67[a,d,e]
Fe-Illite	6.29E-5[d]	6.29E-8[d]	3.15E-13[d]	5.0[d]	8.8[d]	0.60[d]	−0.60[d]	46[a,d,e]	14[a,d,e]	67[a,d,e]
Al-Illite	6.29E-5[d]	6.29E-8[d]	3.15E-13[d]	5.0[d]	8.8[d]	0.60[d]	−0.60[d]	46[a,d,e]	14[a,d,e]	67[a,d,e]
Smectite	3.30E-4[b]	5.23E-6[b]	9.52E-10[b]	5.3[b]	9.4[b]	0.34[b]	−0.40[b]	23.6[b]	35[b]	58.9[b]
Dolomite	2.03E+4[b]	9.31E-1[b]	9.31E-10[a]	8.7[b]	11.0[a]	0.50[b]	0[a]	36.1[b]	52.2[b]	52.2[a]
Chamosite	1.58E-2[c]	9.97E-6[c]	6.29E-10[c]	6.0[c]	9.5[c]	0.53[c]	−0.44[c]	66.5[f]	45[a]	66.5[b]
Clinochlore	2.44E-4[b]	2.18E-6[b]	4.35E-8[b]	6[a]	8[a]	0.26[b]	−0.2[b]	88.0[b]	93.41[b]	93.4[b]
65 °C										
Quartz	1.64E-2	1.06E-4	2.86E-7							
K-Feldspar	3.24E-2	7.54E-5	1.77E-12							
Albite	4.85E-2	2.42E-4	2.34E-7							
Anorthite	2.20E+4	5.59E-2	2.34E-7							
Muscovite	1.27E-4	2.54E-6	2.54E-7							
Annite	1.31E-2	2.54E-5	2.54E-7							
Phlogopite	1.27E-4	4.99E-5	2.54E-7							
Calcite	3.16E+7	1.50E+2	1.50E+2							
Mg-Illite	5.65E-4	1.23E-7	7.71E-12							
Fe-Illite	5.65E-4	1.23E-7	7.71E-12							
Al-Illite	5.65E-4	1.23E-7	7.71E-12							
Smectite	1.02E-3	2.78E-5	1.58E-8							
Dolomite	1.14E+5	1.12E+1	1.12E+1							
Chamosite	3.77E-1	8.54E-5	1.50E-8							
Clinochlore	1.63E-2	1.88E-4	3.75E-6							

[a] These values are assessed by the authors.
[b] Palandri and Kharaka (2004).
[c] Lowson et al. (2005).
[d] Köhler et al. (2003).
[e] Tang and Martin (2011).
[f] Brandt et al. (2003).

(Scheiber et al., 2013). As the brine pH observed in the study of Sanjuan et al. (2010) did not significantly vary beyond a depth of 3600 m, we can consider the pH value constant over a wide range of depth. The CO_2 partial pressure is estimated by the equilibrium calculations reported by Sanjuan et al. (2006).

2.4. Input data

Thermodynamic data for hydrolysis reactions at 65 °C of 15 primary minerals and 7 potential secondary minerals are presented in Table 4. These data are obtained from the Thermoddem database (Blanc et al., 2012). The choice of potential secondary minerals may have significant impacts on the dissolution of primary minerals (Gaucher and Blanc, 2006). The secondary minerals were chosen based on the literature review studies focused on fluid-rock interactions in the context of enhanced geothermal systems. The accuracy of thermodynamic data has an important impact on the output predictions (Savage et al., 2007; Zhu and Lu, 2009; Ngo et al., 2016).

It is well known that kinetic data for minerals are much less available than thermodynamic data, especially for precipitation of mineral phases. Because of this common issue in geochemical modelling works, in the current study, the kinetic approach is used for 15 primary minerals only, and all secondary-formed minerals are precipitated at thermodynamic equilibrium. Table 5 presents the kinetic data of the dissolution reactions for the primary minerals at 25 °C and 65 °C. The

practical application of mineral dissolution requires us to know various parameters for each primary mineral, such as the reaction rate constant and reaction orders with respect to the pH of the solution. The collection of kinetic data of the dissolution processes at 65 °C for all 15 primary minerals is a big issue due to the limited data at high temperatures. Therefore, the data at 65 °C presented in this section were extrapolated from the data proposed by Palandri and Kharaka (2004) using the kinetic data at 25 °C and activation energy terms.

In the kinetic approach of mineral dissolution, the reactive surface area of a mineral is used, as seen in Eq. (6), given that it is a sensitive parameter for the modelling of a geochemical system. Unfortunately, the accuracy of the estimation for this key parameter is often questionable because some important factors are not considered, such as surface roughness and the presence of open pores. Moreover, surface area can change following the progression of the reaction, e.g., temporarily increase if dissolution causes significant surface roughness or decrease when grains are dissolved or become covered by secondary minerals. Thus, the surface area becomes one of the most important uncertainties in dissolution studies (Savage et al., 2002). In the literature, modellers may estimate the reactive surface area with the Brunauer, Emmett and Teller (BET) method (Brunauer et al., 1938; e.g Fagerlund, 1973), the edge site or the geometric surface area. In this work, the reactive surface of 15 primary minerals was estimated from their BET surface areas, assuming that they are proportional to the reactive surface areas. The reactive surface areas corresponding to the
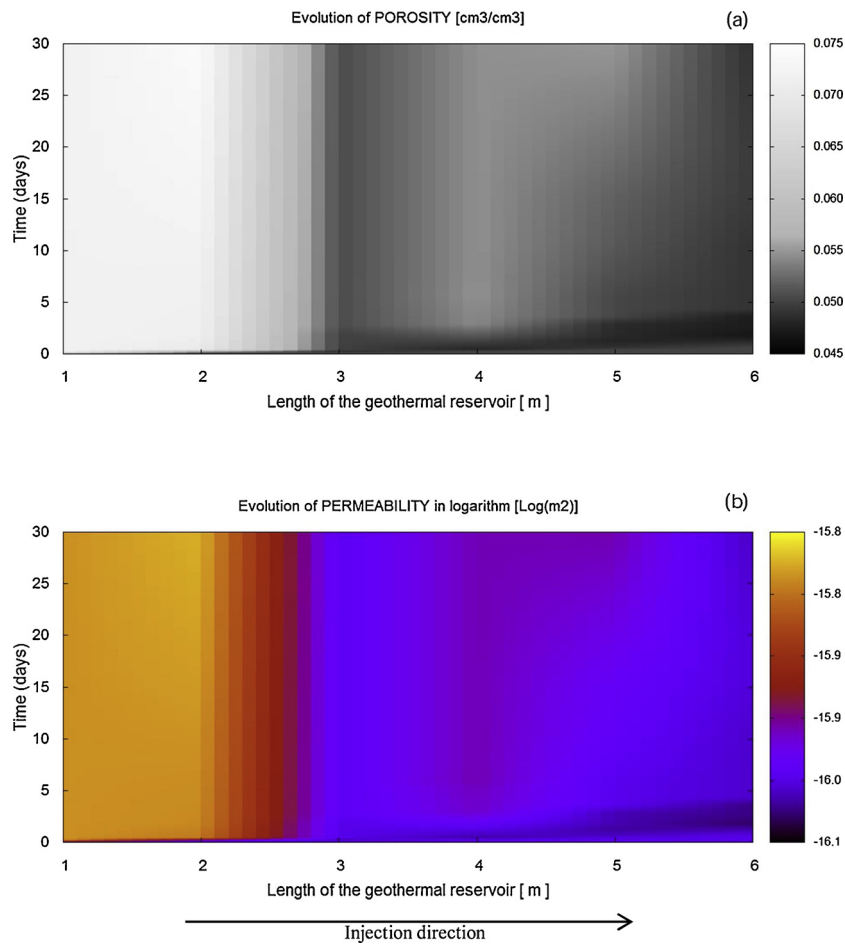
Fig. 2. Calculated spatio-temporal evolution of (a) porosity and (b) permeability in the Soultz geothermal reservoir in the reference case. Permeability is presented with units in logarithm.
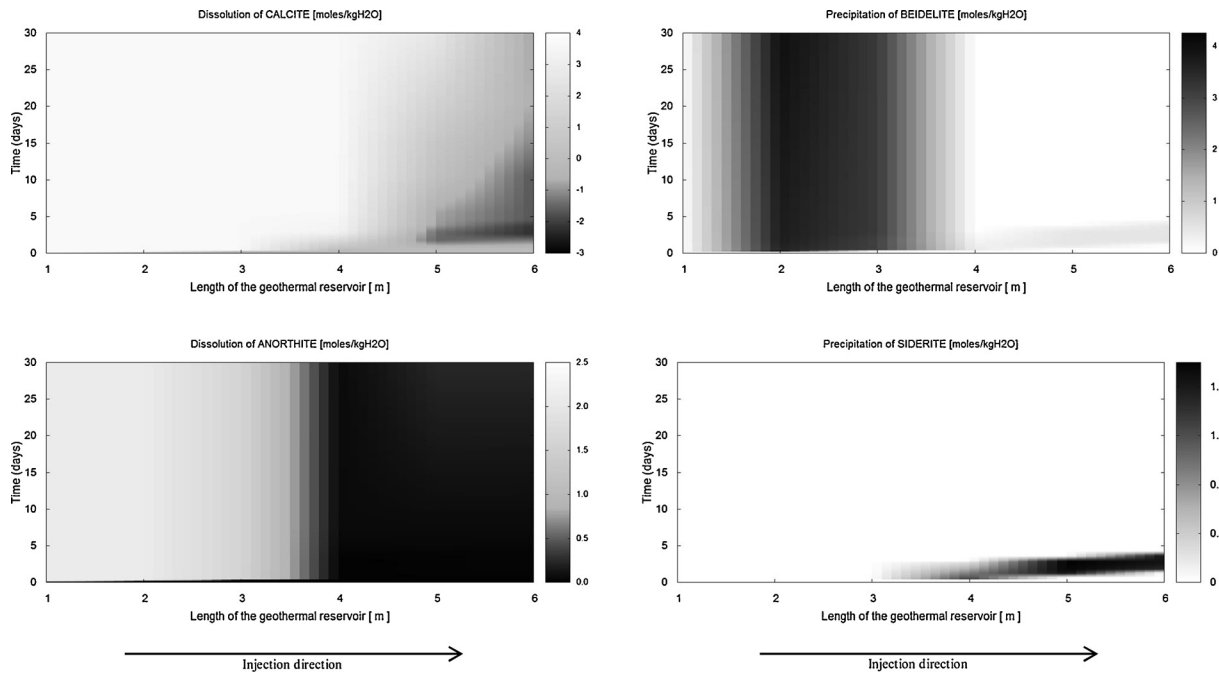

Fig. 3. Calculated spatio-temporal evolution of minerals that are strongly changed. Calcite and anorthite are mainly dissolved. Beidellite and siderite are mainly precipitated. The evolution of these minerals is presented with units of moles/kgH$_2$O.

single and double porosity models are presented in Tables 1 and 2, respectively.

3. Results

3.1. Single porosity model

3.1.1. Reference case

The final porosity and permeability profiles are shown in Fig. 2. In terms of porosity, the initial porosity of the system is assumed to be 0.05, but the porosity scale shown in Fig. 2a varied from 0.045 to 0.075. This is because the stimulation resulted in temporally precipitating carbonates, which caused a temporal closing of the system. However, the increase of porosity from its initial value of 0.05 to the final value of approximately 0.075, occurred mainly within the zone in direct contact with the injection well, and the porosity is open mainly in the zone of 3 m around the injection well. There are only small changes in porosity in the rest of the system. The change in porosity is related to the dissolution of primary minerals and the precipitation of secondary minerals occurring in the system. Similarly, permeability also increases in the system from the initial value of 1.00 to $1.53\ 10^{-16}\ m^2$, mainly in the zone of 3 m around the injection well, similar to the porosity increase. It increases less significantly in the rest of the system. The changes in porosity and permeability strongly depend on each other, because the evolution of permeability is also closely related to the mineralogical transformations.

Unfortunately, the modelling indicates that acid stimulation results in both the dissolution and precipitation of several minerals in the system. The evolution of significantly transformed minerals is presented in Fig. 3. The acid stimulation results are seen for dissolving minerals such as calcite and anorthite, whereas minerals such as beidellite and siderite are locally and temporally precipitated. The dissolution of other minerals such as clay minerals, silicates and oxides remains low.

Calcite (Fig. 3a) is strongly influenced by the acid stimulation. The dissolved amount of calcite varied from -3 to 4 mol kg_{H2O-1}. The modelling results indicate that calcite is quickly dissolved when the acid solution fluids enter into the geothermal reservoir, especially in the zone near the acid-injected well. The dark grey zone in Fig. 3a corresponds to negative values of the dissolution, which means that calcite is precipitated as well. However, this newly formed fraction is mostly re-dissolved at the end of the simulation. With respect to anorthite (Fig. 3b), this mineral is also significantly dissolved under the attack of the acid solution (Fig. 3b), especially in the zone of approximately 3.5 m around the injection well. Its dissolution amount reached 2.5 mol kg_{H2O-1}. Two minerals (beidellite and siderite) are also precipitated in this system. Beidellite (Fig. 3c) is significantly precipitated in the zone approximately 2–3 metres around the injection well. Its precipitation amounts reach 4 mol.kg_{H2O}^{-1}. This fact can provide unexpected results in acid stimulation because this mineral is not re-dissolved at the end of the simulation, as calcite is. The model further indicates that siderite is locally and temporally precipitated (Fig. 3d), however this mineral is quickly re-dissolved.

It is worth noting that in the current study the precipitation process of minerals is treated using the thermodynamic approach. This approach may have numerous limitations, especially when applying quantitative geochemical modelling to a system that is very complex and scenario-dependent, and a limitedly understood chemical environment, such as the Soultz geothermal system. The precipitation of secondary phases may completely change the system geometry, and hence, the transport characteristics of the Soultz geothermal reservoir. Positive achievements of chemical stimulation can be nullified or even worsened by the precipitation of sparingly soluble minerals (GEIE EMC, 2017).

3.1.2. Sensitivity case studies

The sensitivity results are shown in Figs. 4 and 5. For each

sensitivity case, only the effects on porosity are shown and discussed. It is important to note again that in all sensitivity tests, the input data are the same as in the reference case, except for the tested sensitivity parameter. Furthermore, refer to Fig. 2a for a comparable view with respect to the reference case, where the evolution of porosity for the reference case is shown.

3.1.2.1. Case 1: change of the Darcy velocity. Where the Darcy velocities are equal to 0.1 m.h^{-1}, 0.2 m.h^{-1} and 2 m.h^{-1}, the porosity profiles are presented in Fig. 4a–c, respectively. Where the Darcy velocity is 0.1 m.h^{-1}, meaning the injection rate is ten times lower than the reference case (1 m h^{-1}), the porosity at the end of the simulation ranged from 0.04 to 0.11. Compared to the reference case, the maximum porosity is higher, but the opened zone is only limited to 2 m of depth, meaning 1 m less than in the reference case. It is concluded that the low flow rate injection of chemicals is not a good scenario because it limits the penetration of the acid solution into deeper zones of the geothermal reservoir. Low flow rates of stimulation fluids in fractures can also result in the precipitation of secondary reaction products.

When the Darcy velocity is 0.2 m.h^{-1}, the modelling analysis results indicate that the porosity varied from 0.045 to 0.075, and the open zone is limited to 3 m. The porosity in the rest of the system, meaning from 3 m to 6 m away from the injection well, is not clearly open. The modelling results are quite similar to the ones in the reference case. When the Darcy velocity of the acid solution is 2 m.h^{-1}, the porosity at the end of the simulation is in the range of 0.045 to 0.075, and the porosity is open up to 3 m around the injection well. It is found that the modelling results are again quite similar to those of the reference case.

3.1.2.2. Case 2: increase of the injection duration by a factor 2. The evolution of porosity at the end of the simulation is presented in Fig. 5a: the maximum porosity is 0.11, compared to 0.075 in the reference case. The simulated impact zone in this case is limited to 3 m, which is similar to the reference case.

3.1.2.3. Case 3: increase of the acid concentration. For this case, the corresponding results with respect to the final porosity profile are shown in Fig. 5b. The evolution of porosity is quite different from that of the reference case. The results indicate that when the pH of the tested acid solution is 0, the porosity in the impacted zone of the system opens significantly and can reach 0.35, compared to 0.075 in the reference case. Unfortunately, from 2 to 6 m away from the injection well, the porosity decreases drastically. This can be explained by the fact that the higher concentration of the acid solution induced a stronger dissolution of minerals such as calcite and anorthite in the zone in direct contact with the injection well but also by the stronger precipitation of secondary minerals such as beidellite in the rest of the system. One may conclude that when applying a highly concentrated HCl solution, these non-desirable secondary reactions are strongly produced. This reduced the positive achievements of chemical stimulation.

3.1.2.4. Case 4: increase of the initial amount of calcite in the reservoir. Fig. 5c shows the final porosity profile when the initially presented calcite amount is 2 %, compared to 0.46 % in the reference case. Note that the other input parameters are the same as in the reference case. It can be seen in Fig. 5c that the simulated porosity varies from 0.04 to 0.11, which means that the maximum porosity is slightly higher than in the reference case in the zone in direct contact with the injection well; but, in the rest of the system, the porosity is unfortunately closed slightly more strongly than in the reference case. Once again, the impacted zone is always limited to 3 m around the injection well. In this case, the higher initial amount of calcite induces a significantly higher amount of dissolution processes, which, in turn, induces the higher porosity.
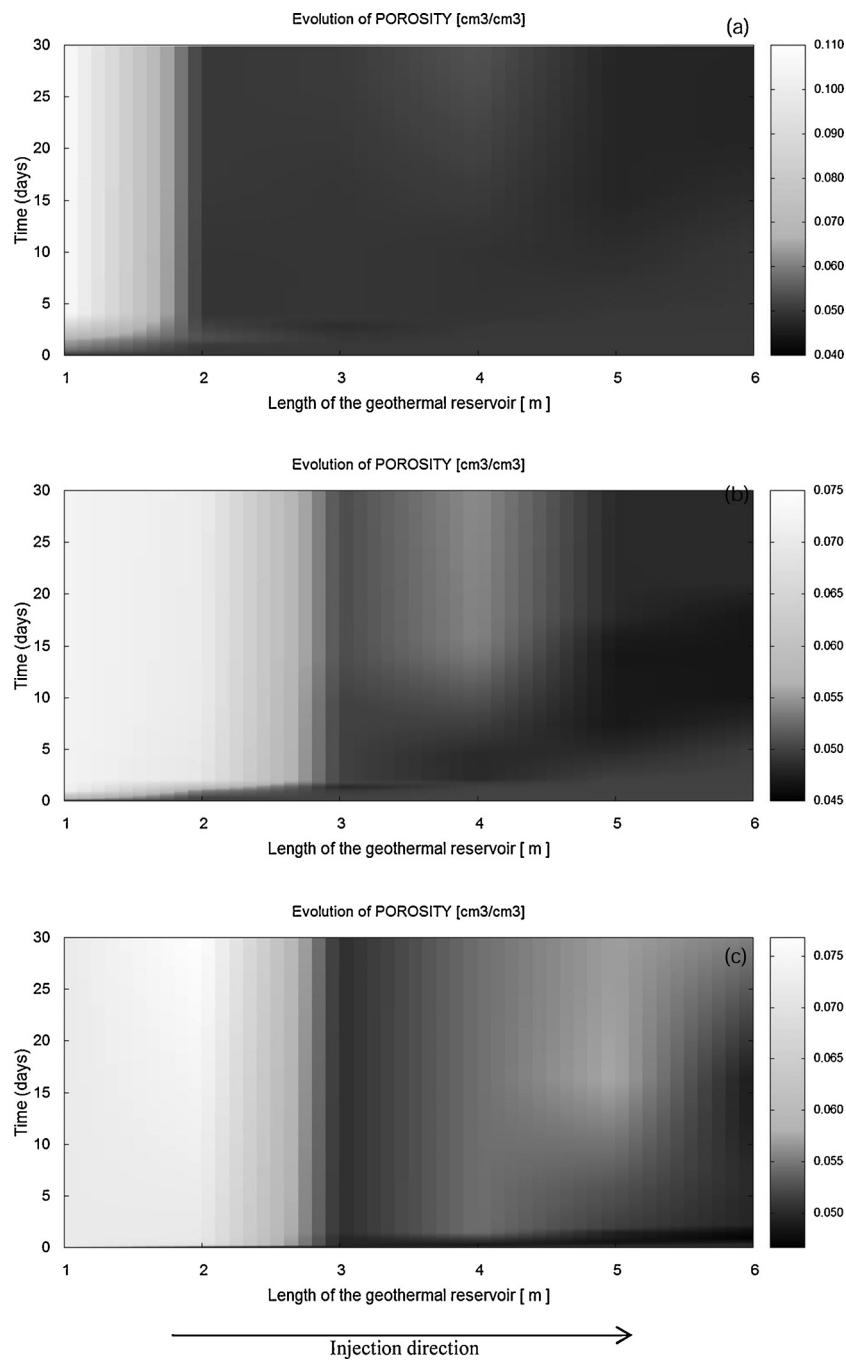
Fig. 4. Calculated spatio-temporal evolution of porosity in the Soultz geothermal reservoir when the Darcy velocity is changed. (a) a Darcy velocity of 0.1 m/h; (b) a Darcy velocity of 0.2 m/h and (c) a Darcy velocity of 2 m/h.

3.2. Double porosity model

Fig. 6 shows the porosity profiles of the Soultz geothermal reservoir after 30 days of acid stimulation. Note again that in this model, we use different input data in terms of the mineralogical composition and the physical properties of the system. Similar to different cases of the single porosity model presented in detail in previous sections, the simulated porosity in the geothermal reservoir is divided into two zones. As expected, the zone in contact with the injection well is more significantly opened than in the previous case, where the model used assumes that the system is homogeneous. For this model, the maximum porosity reaches values of 0.16 and 0.14 when the ratio of surface contact and volume contact between the fracture and matrix zones are 1000 and 10,000, respectively. It is not expected that in both cases of the double

porosity model, the porosity of the rest of the system is very low. This also means that the stronger opening in the zone in direct contact also induces the stronger decrease of porosity in the rest of the system.

4. Discussion

4.1. Single porosity model

The modelling of the acid stimulation in different scenarios reveals that the evolution of porosity and permeability of the Soultz geothermal reservoir in direct contact with the injection well are significantly influenced by the Darcy velocities and the initial conditions of the acid solutions used. The modelling analysis results indicate that mineralogical transformations of minerals within the system controlled the
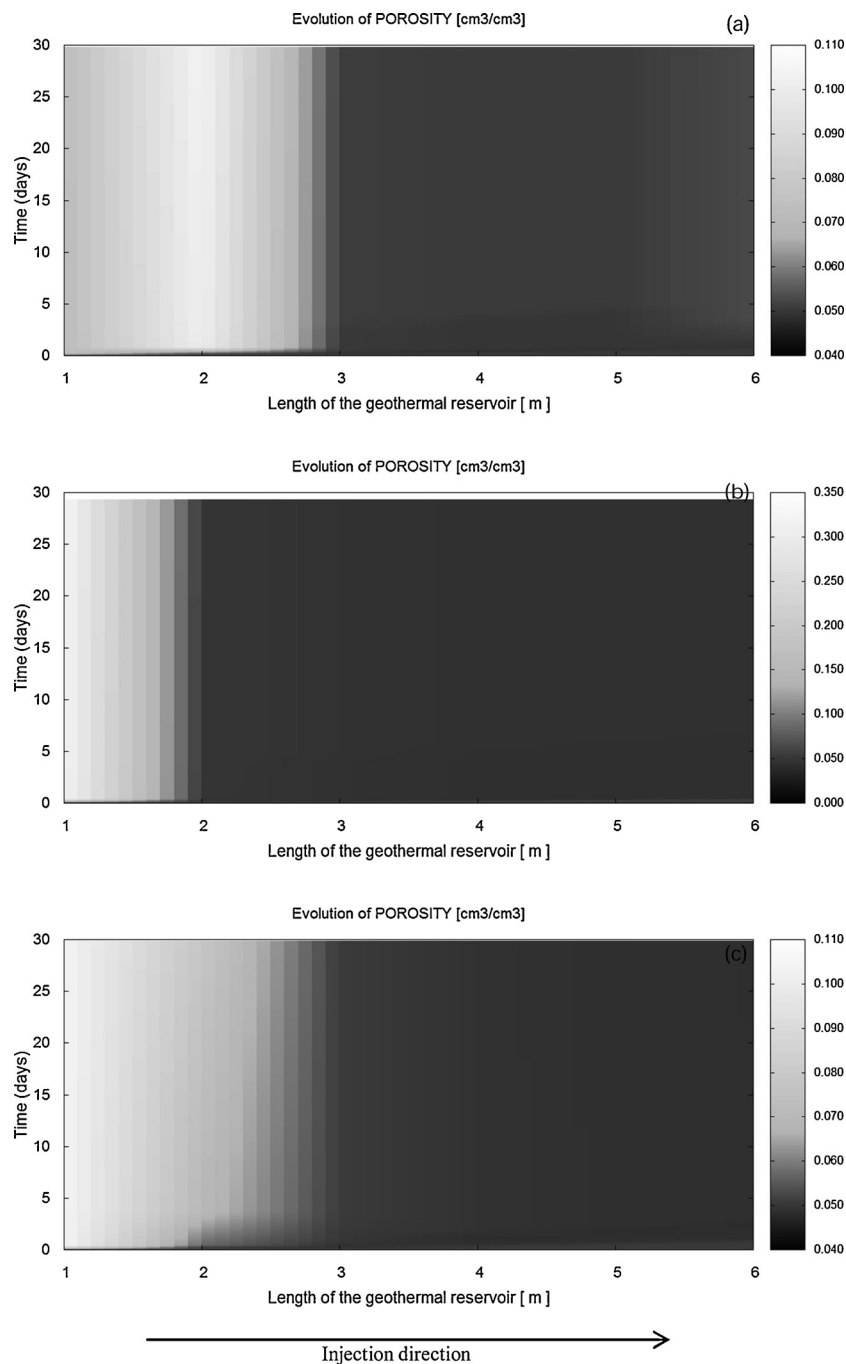
Fig. 5. Calculated spatio-temporal evolution of porosity in the Soultz geothermal reservoir under different scenarios. (a) increase of the injection duration by a factor of 2; (b) increase of the acid concentration, pH = 0 nd (c) increase of the calcite quantity that is initially present in the reservoir.

evolution of the geothermal reservoir during the acid stimulation. These transformations are mainly related to the dissolution of minerals such as calcite and anorthite and to the precipitation of secondary formed minerals such as beidellite. The zone in direct contact with the injected acid solution is mostly open. The porosity increases from the initial value of 0.05 to a value of 0.35, similar to the modelling case where the volume of the injected acid solution increased two-fold. However, the impacted zone is always limited to a few metres around the injected acid stimulation.

It is recognized that the dissolution of primary minerals is governed by numerous factors that can have direct impacts on the dissolution of minerals. For example, in the case of calcite, its dissolution rate is controlled by many parameters, including the dissolution constant, the

reactive surface area, the pH of the aqueous solution, and the temperature. In the current study, only a few scenarios are reported in detail. We can learn various lessons from these tests. The strong reaction rate of the interaction between the HCl solution and calcite induces an intense mineralogical transformation and therefore an important increase of porosity in the zone close to the acid injection well. However, this in turn limits the diffusion of the acid solution towards deeper zones of the system. The porosity decrease in the rest of the system is, therefore, a secondary effect that is not expected at all.

We can therefore acknowledge the key role of the Darcy velocity of the acid stimulation on the evolution of the geothermal reservoir at the end of the simulation. Unfortunately, the acid stimulation also induced temporal and local closing of the system because of the strong
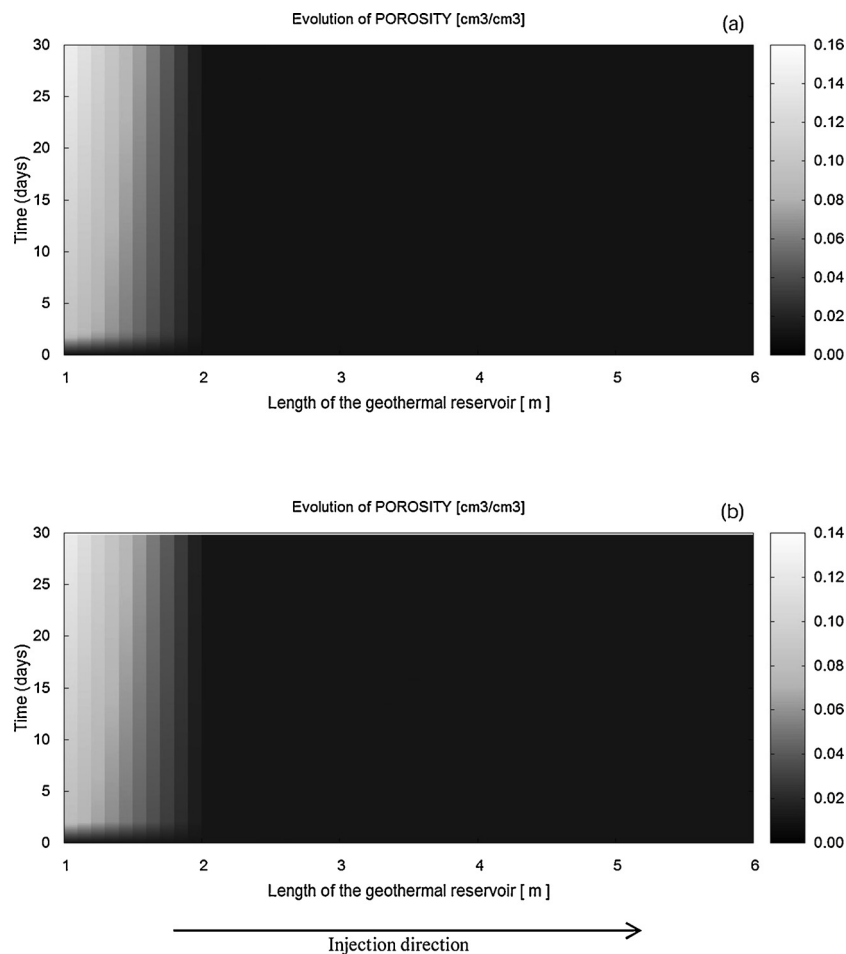
Fig. 6. Calculated spatio-temporal evolution of porosity in the Soultz geothermal reservoir when using the double porosity model. The ratio of surface contact and volume contact between fractured and matrix zones are (a) 1000 and (b) 10,000.

precipitation of secondary minerals. It is clear that a strong acid such as HCl, in combination with a low flow rate, produces not only many reaction products near the acid injected well in a short time but also causes these products to accumulate due to poor hydraulic conditions. In addition, precipitation of less soluble minerals will occur in the rest of the system. For future attempts at acid stimulation, on one hand, the accumulation of reaction products needs to be avoided, but on the other hand, a certain contact time for mineral dissolution is required for optimal efficiency.

4.2. Double porosity model

The use of the double porosity model shows a clear difference in the evolution of the porosity at the end of the simulation. The analysis of the porosity profile confirms the higher increase of porosity in the zone in direct contact with the injected acid solution.

In this modelling study, the initial volumes of calcite present in the geothermal reservoir are 0.3 % and 3.9 % for the matrix and fracture, respectively. The initial quantity in the fracture is in the range of those reported in the literature for the Soultz geothermal reservoir (e.g., Ledésert et al., 2009, 2010; Hébert et al., 2010). The literature review also shows that the mineralogical composition of the Soultz geothermal reservoir is very heterogeneous and there is a large range of carbonate present in the reservoir. It is found that the carbonate's quantity in the fractures strongly depends on the interaction between the brine solution and the geothermal reservoir. Unfortunately, the precise determination of the mineralogical composition of the geothermal reservoir is a great challenge. Therefore, the amount of calcite used in the present

study was selected to be in the range found from the literature review (e.g., Ledésert et al., 2009, 2010; Hébert et al., 2010).

Furthermore, the initial porosity of the system is potentially important for the modelling outputs. However, with the very limited availability of data, we have to assume that the porosity values in the matrix and fractures zones are 10 % and 1 %, respectively, in a simplified conceptual system. We acknowledge that these values are questionable compared to the variability of the Soultz geothermal reservoir. Nevertheless, the modelling results suggest that the accuracy in the determination of the input data for the Soultz geothermal reservoir and the real conditions of the system may control the modelling results of the evolution of the geothermal reservoir after acid stimulation. The experimental determination of the initial conditions related to the Soultz geothermal reservoir is still very limited, but this is expected to improve the quality of the modelling work, especially in the framework of the enhanced geothermal system.

4.3. The choice of acid solution

HCl acid is strong, effective, inexpensive, temperature stable, and its reaction rate increases with temperature. However, this acid may have several negative aspects in terms of the reactions. In the context of the Soultz geothermal system, it can be found from this modelling work that unwelcome secondary reactions are produced. This can happen when highly concentrated HCl is used or if low flow rate conditions are applied to the acid stimulation. The precipitation of secondary formed minerals can reduce the positive achievements of chemical stimulation.

In the last several years, public interest and discussion concerning

the environmental impacts of chemical treatment in deep-seated formations has grown. This leads to an increasing amount of demand for mining and water authorities to use environmentally friendly and biodegradable chemicals. In addition, the demand for highly sophisticated chemical mixtures that are able to target different types of minerals is continuously attributed to the management of geothermal systems. Recently, environmentally friendly and biodegradable acids and chelating agents are increasingly used for acidizing operations, especially in the areas where wells are shallow or close to water protection areas (GEIE EMC, 2017). However, this is not the case for the Soultz geothermal system. The new formulations of chemical mixtures are very effective, combining acids and chelating agents, or even chemical systems at a moderate pH that do not contain acids. Their ability to dissolve various minerals such as sulfates, sulfides, clay minerals and carbonates make them unique and thus, they are appropriate for unconventional reservoir acidizing. Their successful applications in the Upper Rhine Graben have already been shown (Lummer et al., 2015, Baujard et al., 2017).

The literature review shows that acid stimulation usually affects the near-field region around the well. In the Soultz geothermal reservoir, it is considered to reach a maximum diameter of 6 m around the well. Since chemical stimulations often apply to a small volume compared to hydraulic stimulations, they would not affect reservoir volumes as much as hydraulic stimulation. The positive achievement for the near-field region around the well obtained from the acid stimulation is then considered as a "door-opener" that prepares slightly permeable fracture zones for further hydraulic stimulation. The GPK-4 injection well has not been put into full operation yet due to its low injectivity. Therefore, the successful application of acid stimulation in this injection well could result in an increase of power plant economics and would further lower the potential for induced seismicity related to brine circulation.

5. Conclusions

The modelling of acid stimulation in the Soultz geothermal reservoir was conducted by using the KIRMAT code. The acid stimulation of the Soultz-sous-Forêts system was built with the assumption that the GKP-4 injection well and a simple acid such as HCl were chosen for the coming stimulation campaign. The calculation was simulated by two types of models: the single porosity and double porosity models.

In the single porosity model, the simulated results for the reference case explored an increase in porosity, resulting from a strong dissolution of the primary minerals such as calcite and anorthite in the zone around the acid-injected well. However, there is also a precipitation of secondary minerals such as beidellite, which leads to a porosity decrease in the rest of the system. It is concluded that the evolution of porosity and permeability in the Soultz system is mainly impacted by the dissolution of primary minerals, especially for a strong transformation of calcite and anorthite and for the formation of second minerals such as beidellite. The modelling results obtained from the sensitivity study cases show the significant impacts of the Darcy velocity, the initial concentration of the used acid, the duration of the injection and the initially presented calcite amount, and especially, the changes in porosity and the mineralogical transformation in the zone around the acid-injected well. The higher concentration of the HCl solution also increased the dissolution of the primary minerals and subsequently produced a stronger increase of the porosity in the zone around the injection well. It was further found that when applying a highly concentrated HCl solution, unwelcome secondary reactions are strongly produced. This unexpected precipitation reduces the positive achievements of chemical stimulation. Additionally, the quick reaction between the HCl solution and the primary minerals in the system limit the transport of the acid solution into further zones of the system, and this resulted in a very narrowly impacted zone around the acid-injected well.

The use of the double porosity model indicates a significant difference in the evolution of porosity in the system. The strong opening of the porosity is also mainly related to the dissolution of calcite and the formation of secondary minerals. The comparison of the modelling results by the single porosity and double porosity models confirm that the impacted zone is limited to a few metres around the acid-injected well.

Numerous factors were found to have impacts on the modelling outputs of the acid stimulation. The accuracy of the predicted results is likely related to possessing accurate knowledge about the conditions of the Soultz geothermal reservoir. Even though various experimental and modelling works have been carried out, the determination *in situ* of the reservoir is still very limited due to various challenges. In the future, more knowledge of the geothermal reservoir is needed to improve the accuracy of the modelling output.

Declaration of Competing Interest

The authors declare that they have no known competing financial interests or personal relationships that could have appeared to influence the work reported in this paper.

Acknowledgements

References

Ackerer, J., Chabaux, F., Lucas, Y., Clément, A., Fritz, B., Beaulieu, E., Viville, D., Pierret, M.C., Gangloff, S., Négrel, Ph, 2018. Monitoring and reactive-transport modeling of the spatial and temporal variations of the Strengbach spring hydrochemistry. Geochim. Cosmochim. Acta 225, 17–35.

Aichholzer, C., Duringer, P., Orciani, S., Genter, A., 2016. New stratigraphic interpretation of the Soultz-sous-Forêts 30-year-old geothermal wells calibrated on the recent one from Rittershoffen (Upper Rhine Graben, France). Geotherm. Energy 4 (1), 13.

André, L., Rabemanana, V., Vuataz, F.D., 2006. Influence of water-rock interactions on fracture permeability of the deep reservoir at Soultz-sous-Forêts, France. Geothermics 35 (5–6), 507–531.

Bächler, D., Kohl, T., 2005. Coupled thermal-hydraulic-chemical modelling of enhanced geothermal systems. Geophys. J. Int. 161 (2), 533–548.

Baldeyrou-Bailly, A., Surma, F., Fritz, B., 2004. Geophysical and mineralogical impacts of fluid injection in a geothermal system: The Hot Fractured Rock site at Soultz-sous-Forêts, France. Geol. Soc. Spec. Publ. 236, 355–367.

Baldeyrou, A., Vidal, O., Fritz, B., 2003. Experimental study of phase transformation in a thermal gradient; Application to the Soultz-sous-Forêts granite (France). Comptes Rendus - Geoscience 335 (4), 371–380.

Bartier, D., Ledésert, B., Clauer, N., Meunier, A., Liewig, N., Morvan, G., Addad, A., 2008. Hydrothermal alteration of the Soultz-sous-Forêts granite (Hot Fractured Rock geothermal exchanger) into a tosudite and illite assemblage. Eur. J. Mineral. 20 (1), 131–142.

Blanc, P., Lassin, A., Piantone, P., Azaroual, M., Jacquemet, N., Fabbri, A., Gaucher, E.C., 2012. Thermoddem: a geochemical database focused on low temperature water/rock interactions and waste materials. Appl. Geochem. 27 (10), 2107–2116.

Brandt, F., Bosbach, D., Krawczyk-Bärsch, E., Arnold, T., Bernhard, G., 2003. Chlorite dissolution in the acid pH-range: a combined microscopic and macroscopic approach. Geochim. Cosmochim. Acta 67 (8), 1451–1461.

Brunauer, S., Emmett, P.H., Teller, E., 1938. Adsorption of gases in multimolecular layers. J. Am. Chem. Soc. 60 (2), 309–319.

Dezayes, C., Genter, A., Hooijkaas, G.R., 2005. Deep-seated geology and fracture system of the EGS Soultz reservoir (France) based on recent 5km depth boreholes. Proceedings World Geothermal Congress.

Dubois, M., Ledésert, B., Potdevin, J.L., Vançon, S., 2000. Determination of the formation conditions of carbonates in an alteration zone of the Soultz-sous-Forets granite (Rhine Graben): The fluid inclusion record. Comptes Rendus de l'Academie de Sciences - Serie IIa: Sciences de la Terre et des Planetes 331 (4), 303–309.

Dubois, M., Ougougdal, M.A., Meere, P., Royer, J.J., Boiron, M.C., Cathelineau, M., 1996. Temperature of paleo- to modern self-sealing within a continental rift basin : The fluid inclusion data (Soultz-sous-Forêts, Rhine graben, France). Eur. J. Mineral. 8 (5), 1065–1080.

Fagerlund, G., 1973. Determination of specific surface by the BET method. Matériaux et Construction 6 (3), 239–245.

Fritz, B., Jacquot, E., Jacquemont, B., Baldeyrou-Bailly, A., Rosener, M., Vidal, O., 2010. Geochemical modelling of fluid-rock interactions in the context of the Soultz-sous-Forêts geothermal system. Comptes Rendus - Geoscience 342 (7–8), 653–667.

Gaucher, E.C., Blanc, P., 2006. Cement/clay interactions–a review: experiments, natural analogues, and modeling. Waste Manag. 26 (7), 776–788.

GEIE EMC, 2017. DESTRESS – Feasibility Study: Chemical Stimulation of an Injection Well at Soultz-sous-Forêts - France. GEIE EMC confidential report, Kutzenhausen, pp. 75.

Genter, A., Traineau, H., 1992. Borehole EPS-1, Alsace, France: preliminary geological results from granite core analyses for Hot Dry Rock research. Sci. Drill. 3 (5), 205–214.

Genter, A., Evans, K., Cuenot, N., Fritsch, D., Sanjuan, B., 2010. Contribution of the exploration of deep crystalline fractured reservoir of Soultz to the knowledge of enhanced geothermal systems (EGS). Comptes Rendus - Geoscience 342 (7-8), 502–516.

Gérard, F., 1996. Modélisation géochimique thermodynamique et cinétique avec prise en compte des phénomènes de transport de masse en milieu poreux saturé (PhD Thesis). pp. 150. Université de Strasbourg.

Gérard, F., Clement, A., Fritz, B., 1998. Numerical validation of a Eulerian hydrochemical code using a 1D multisolute mass transport system involving heterogeneous kinetically controlled reactions. J. Contam. Hydrol. 30 (3), 201–216.

Haas, I.O., Hoffmann, C.R., 1929. Temperature gradient in pechelbronn oil-bearing region, Lower Alsace: its determination and relation to oil reserves. AAPG Bull. 13 (10), 1257–1273.

Heap, M.J., Kushnir, A.R., Gilg, H.A., Wadsworth, F.B., Reuschlé, T., Baud, P., 2017. Microstructural and petrophysical properties of the Permo-Triassic sandstones (Buntsandstein) from the Soultz-sous-Forêts geothermal site (France). Geotherm. Energy 5 (1), 26.

Hébert, R., Ledésert, B., Genter, A., Bartier, D., Dezayes, C., 2011. Mineral precipitation in geothermal reservoir: the study case of calcite in the Soultz-sous-Forêts enhanced geothermal system. 36rd Workshop on Geothermal Reservoir Engineering pp. SGP-TR-191.

Hébert, R.L., Ledésert, B., 2012. Calcimetry at soultz-sous-forêts enhanced geothermal system: relationships with fracture zones, flow pathways and reservoir chemical stimulation results. Geotherm. Energy Technol. Geol. 93–113.

Hébert, R.L., Ledésert, B., Bartier, D., Dezayes, C., Genter, A., Grall, C., 2010. The enhanced geothermal system of soultz-sous-forêts: A study of the relationships between fracture zones and calcite content. J. Volcanol. Geotherm. Res. 196 (1–2), 126–133.

Jacquot, E., 2000. Modélisation thermodynamique et cinétique des réactions géochimiques entre fluides de bassin et socle cristallin: application au site expérimental du programme européen de recherche en géothermie profonde (Soultz-sous- Forêts, Bas-Rhin, France). Louis Pasteur University.

Köhler, S.J., Dufaud, F., Oelkers, E.H., 2003. An experimental study of illite dissolution kinetics as a function of ph from 1.4 to 12.4 and temperature from 5 to 50°C. Geochim. Cosmochim. Acta 67, 3583–3594.

Komninou, A., Yardley, B.W.D., 1997. Fluid-rock interactions in the Rhine Graben: a thermodynamic model of the hydrothermal alteration observed in deep drilling. Geochim. Cosmochim. Acta 61 (3), 515–531.

Ledésert, B., Berger, G., Meunier, A., Genter, A., Bouchet, A., 1999. Diagenetic-type reactions related to hydrothermal alteration in the Soultz-sous-Forets granite. France. European Journal of Mineralogy 11 (4), 731–741.

Ledésert, B., Dubois, J., Genter, A., Meunier, A., 1993a. Fractal analysis of fractures applied to Soultz-sous-Forets hot dry rock geothermal program. J. Volcanol. Geotherm. Res. 57 (1–2), 1–17.

Ledésert, B., Dubois, J., Velde, B., Meunier, A., Genter, A., Badri, A., 1993b. Geometrical and fractal analysis of a three-dimensional hydrothermal vein network in a fractured granite. J. Volcanol. Geotherm. Res. 56 (3), 267–280.

Ledésert, B., Hebert, R., Genter, A., Bartier, D., Clauer, N., Grall, C., 2010. Fractures, hydrothermal alterations and permeability in the Soultz enhanced Geothermal System. Comptes Rendus – Geoscience 342 (7–8), 607–615.

Ledésert, B., Hébert, R.L., Grall, C., Genter, A., Dezayes, C., Bartier, D., Gérard, A., 2009. Calcimetry as a useful tool for a better knowledge of flow pathways in the Soultz-sous-Forêts Enhanced Geothermal System. J. Volcanol. Geotherm. Res. 181 (1–2), 106–114.

Lichtner, P.C., 1988. The quasi-stationary state approximation to coupled mass transport and fluid-rock interaction in a porous medium. Geochim. Cosmochim. Acta 52 (1), 143–165.

Lowson, R.T., Comarmond, M.C.J., Rajaratnam, G., Brown, P.L., 2005. The kinetics of the dissolution of chlorite as a function of pH and at 25 C. Geochim. Cosmochim. Acta 69

(7), 1687–1699.

Lucas, Y., Chabaux, F., Schaffhauser, T., Fritz, B., Ambroise, B., Ackerer, J., Clément, A., 2017. Hydrogeochemical modeling (KIRMAT) of spring and deep borehole water compositions in the small granitic Ringelbach catchment (Vosges Mountains, France). Appl. Geochem. 87, 1–21.

Marty, N.C.M., Tournassat, C., Burnol, A., Giffaut, E., Gaucher, E.C., 2009. Influence of reaction kinetics and mesh refinement on the numerical modelling of concrete/clay interactions. J. Hydrol. 364 (1–2), 58–72. https://doi.org/10.1016/j.jhydrol.2008.10.013.

Nami, P., Schellschmidt, R., Schindler, M., Tischner, R., 2008. Chemical stimulation operations for reservoir development of the deep crystalline HDR/EGS system at Soultz-sous-Forêts (France). In: Proceedings of the 32nd Workshop on Geothermal Reservoir Engineering. Stanford University, Stanford, CA, USA. pp. 5.

M'Nassri, S., Lucas, Y., Schäfer, G., Dridi, L., Majdoub, R., 2019. Coupled hydro-geochemical modelling using KIRMAT to assess water-rock interaction in a saline aquifer in central-eastern Tunisia. Appl. Geochem. 102, 229–242.

Ngo, V.V., Delalande, M., Clément, A., Michau, N., Fritz, B., 2014. Coupled transport-reaction modeling of the long-term interaction between iron, bentonite and Callovo-Oxfordian claystone in radioactive waste confinement systems. Appl. Clay Sci. 101 (0), 430–443.

Ngo, V.V., Lucas, Y., Clément, A., Fritz, B., 2016. Modeling the impact of temperature on the saturation state and behavior of minerals in the Soultz-sous-Forêts geothermal system. Geothermics 64, 196–208.

Palandri, J.L., Kharaka, Y.K., 2004. A Compilation of Rate Parameters of Water-mineral Interaction Kinetics for Application to Geochemical Modeling (No. OPEN-FILE-2004-1068). .

Portier, S., Vuataz, F.D., Nami, P., Sanjuan, B., Gérard, A., 2009. Chemical stimulation techniques for geothermal wells: experiments on the three-well EGS system at Soultz-sous-Forêts, France. Geothermics 38 (4), 349–359.

Rabemanana, V., Durst, P., Bächler, D., Vuataz, F.D., Kohl, T., 2003. Geochemical modelling of the Soultz-sous-Forêts Hot Fractured Rock systemcomparison of two reservoirs at 3.8 and 5 km depth. Geothermics 32 (4), 645–653.

Sanjuan, B., Millot, R., Dezayes, C., Brach, M., 2010. Main characteristics of the deep geothermal brine (5km) at Soultz-sous-Forêts (France) determined using geochemical and tracer test data. Comptes Rendus Geosci. 342 (7), 546–559.

Sanjuan, B., Pinault, J.L., Rose, P., Gérard, A., Brach, M., Braibant, G., Crouzet, C., Foucher, J.C., Gautier, A., Touzelet, S., 2006. Tracer testing of the geothermal heat exchanger at Soultz-sous-Forêts (France) between 2000 and 2005. Geothermics 35 (5–6), 622–653.

Sausse, J., 2002. Hydromechanical properties and alteration of natural fracture surfaces in the Soultz granite (Bas-Rhin, France). Tectonophysics 348 (1–3), 169–185.

Sausse, J., Fourar, M., Genter, A., 2006. Permeability and alteration within the Soultz granite inferred from geophysical and flow log analysis. Geothermics 35 (5-6), 544–560.

Savage, D., Noy, D., Mihara, M., 2002. Modelling the interaction of bentonite with hyperalkaline fluids. Appl. Geochem. 17 (3), 207–223.

Savage, D., Walker, C., Arthur, R., Rochelle, C., Oda, C., Takase, H., 2007. Alteration of bentonite by hyperalkaline fluids: a review of the role of secondary minerals. Phys. Chem. Earth 32 (1–7), 287–297.

Scheiber, J., Seibt, A., Birner, J., Genter, A., Moeckes, W., 2013. Application of a scaling inhibitor system at the geothermal power plant in Soultz-sous-Forêts: laboratory and on-site studies. In: Proceedings of European Geothermal Congress. Pisa, Italy.

Surma, F., Géraud, Y., 2003. Porosity and thermal conductivity of the Soultz-sous-Forêts granite. Pure Appl. Geophys. 160 (5–6), 1125–1136.

Tang, Y., Martin, S.T., 2011. Siderite dissolution in the presence of chromate. Geochim. Cosmochim. Acta 75 (17), 4951–4962.

Villeneuve, M.C., Heap, M.J., Kushnir, A.R.L., Qin, T., Baud, P., Zhou, G., Xu, T., 2018. Estimating in situ rock mass strength and elastic modulus of granite from the Soultz-sous-Forêts geothermal reservoir (France). Geotherm. Energy 6 (1), 11.

Vogt, C., Marquart, G., Kosack, C., Wolf, A., Clauser, C., 2012. Estimating the permeability distribution and its uncertainty at the EGS demonstration reservoir Soultz-sous-Forêts using the ensemble Kalman filter. Water Resour. Res. 48 (8).

Zhu, C., Lu, P., 2009. Alkali feldspar dissolution and secondary mineral precipitation in batch systems: 3. Saturation states of product minerals and reaction paths. Geochim. Cosmochim. Acta 73 (11), 3171–3200.